

# Model Predictive Current Control of Dual-Mode Voltage Source Inverter Operations: Islanded and Grid-Connected

1<sup>st</sup> Fatima Martinez

*Maestría en Ingeniería Electrónica*  
*Universidad Cono Sur de las Américas*  
Asunción, Paraguay  
fmartinez@alumnomie.ucsa.edu.py

2<sup>nd</sup> Thalia Morel

*Maestría en Ingeniería Electrónica*  
*Universidad Cono Sur de las Américas*  
Asunción, Paraguay  
tmorel@alumnomie.ucsa.edu.py

3<sup>rd</sup> Hector Fretes

*Maestría en Ingeniería Electrónica*  
*Universidad Cono Sur de las Américas*  
Asunción, Paraguay  
hfretes@alumnomie.ucsa.edu.py

4<sup>th</sup> Jorge Rodas

*Universidad Nacional de Asunción*  
Luque, Paraguay  
jrodas@ing.una.py

5<sup>th</sup> Yassine Kali

*École de Technologie Supérieure*  
Montreal, Canada  
y.kali88@gmail.com

6<sup>th</sup> Raul Gregor

*Universidad Nacional de Asunción*  
Luque, Paraguay  
rgregor@ing.una.py

**Abstract**—Model predictive control (MPC) has been a research topic for power converters control due to its simplicity, easy inclusion of constraints, fast dynamic response, among others. This work proposes the use of MPC as a current regulator of a voltage source inverter (VSI) in a dual-mode operation. On one hand, the VSI is used to provide current to a load from a photovoltaic panel, being in islanded condition. On the other hand, the VSI is used as an active power filter for the reactive power compensation for a grid-connected condition. Simulation results are provided to show the benefits of the proposed controller.

**Index Terms**—Active power filter, current control, photovoltaic systems, model predictive control, voltage source inverter.

## NOMENCLATURE

APF	Active power filter.
DG	Distributed generation.
FFT	Fast Fourier transform.
MPC	Model predictive control.
PCC	Predictive current control.
PV	Photovoltaic.
RES	Renewable energy sources.
THD	Total harmonic distortion.
VSI	Voltage source inverter.

## I. INTRODUCTION

In the last years, the renewable energy sources (RES) and power quality have captured the attention of the international scientific community. This has been mainly justified, on the one hand, for the need to meet energy demands, and on the other hand, for the need to optimize the available energy resources [1], [2]. In both applications, power electronic converters play an important role due to this devices are capable of modifying the input voltage and current characteristics in order to interconnect RES with the distribution grid under the concept of distributed

generation (DG), feed an islanded load or improve the power quality [3]. Besides, several new power converter topologies have been proposed in the literature, such as matrix converters [4], [5] multilevel converters [6], [7] neutral-point clamped converter [8], [9] among others, the two-level voltage source inverter (VSI) is still the most used in industry applications [10], [11]. One of the most commonly used three-phase converter topology is based on three H-bridge cells [12].

The design of suitable controllers for power converters applied to DG is an issue of paramount importance to researchers. For the particular case of control of VSIs, different new techniques have been studied and applied in the past decades, such as the sliding-mode control [13], [14], dead-beat control [15], [16], or the model predictive control (MPC) [17], [18], among others. As a consequence of the fast development of digital signal processors, the finite-set MPC has become a promising control method for power converters due to its advantages, such as a fast-tracking response, a high control bandwidth, and providing a very simple way of including system nonlinearities and constraints [19].

This paper proposes the MPC for a complex control strategy with multiple objectives, using the predictive current control (PCC) for a dual-mode VSI operation. Is based on [12] where a PCC was carried out to compensate reactive power in the load as well as to compensate current in the neutral. In this case, the PCC will be applied to the output of the two-level H-bridge converter, in one case working as an active power filter (APF) while, in the other case, to feed a load through the VSI. In both cases, instantaneous measurements are carried out in order to know the reactive power to be compensated, this compensation is carried out by injecting a reactive current that is 180 degrees out of phase proceeding from the reactive power of the system.

In order to guarantee a more continuous system, the converter relies on photovoltaic (PV) panels as the main source of choice for the energy required which has a DC-link to store the energy, whether to compensate reactive power or to supply energy to the load according to its functionality. This control was chosen for the robustness of the MPC control and its effectiveness in controlling the desired parameters [20]. The prediction of the output current is obtained with the actuation of the circuit interrupters that determines the voltage level. The voltage chosen is the one that provides the least error between the measured and the predicted current in the cost function, to achieve the expected follow-up. A cost function has been identified where each specific sector is evaluated at each sampling time, based on controlled variables such as the actual filter voltage [12]. The large take-up of renewable energy-based power generation and integration with the existing energy system introduces energy quality problems, such as harmonics and reliability issues, so the integration of renewable energy with improved energy quality is the current trend in research [21]. A passive filter of first order RL is used at the output to improve the quality of the current, since it is the case of a balanced load is not necessary to use a higher order passive filter [22].

## II. MATHEMATICAL MODEL OF THE SYSTEM

The mathematical model of the system is divided in VSI and APF operation modes. Fig. 1 shows the circuit diagram of both cases of the dual-mode operation of the system under study. On one hand, Fig. 1(a) shows the mode of operation as APF connected to the grid. On the other hand, in case of grid disconnection, it automatically switches to its operation as Islanded VSI, shown in Fig 1(b), where PV panels are used as a power source.

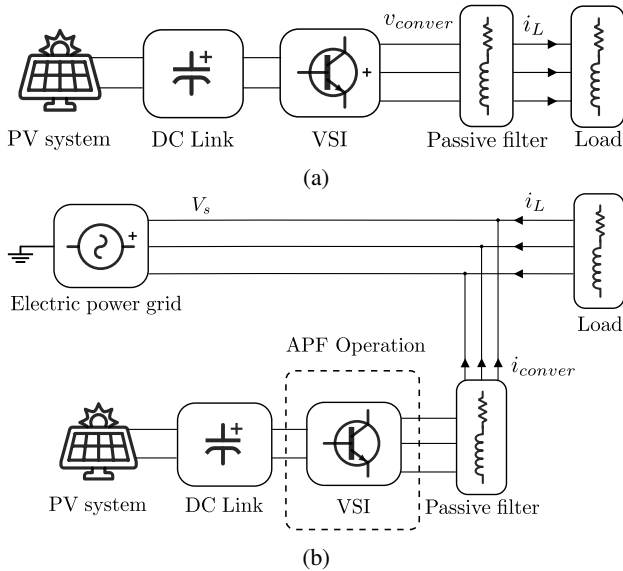


Fig. 1: Scheme of the systems under: (a) Islanded VSI, (b) Grid-Connected APF.

### A. VSI operation mode

By means of Kirchoff's law, for each phase is obtained [23]:

$$v_{R_f} + v_L - v_{conver} + v_{L_f} = 0,$$

$$R_f i_L + v_L - v_{conver} + L_f \frac{d}{dt} i_L = 0, \quad (1)$$

thus,

$$L_f \frac{d}{dt} i_L = v_{conver} - R_f i_L - v_L. \quad (2)$$

The next equation is the discrete form of (2).

$$i_{L[n+1]} = \frac{T_m}{L_f} [v_{conver[n]} - v_{L[n]}] + i_{L[n]} D \quad (3)$$

being

$$D = \left[ 1 - \frac{T_m R_f}{L_f} \right],$$

where  $v_{R_f}$  is the voltage on the passive filter resistor,  $v_{L_f}$  the voltage on the passive filter inductor,  $v_{conver}$  the active power filter voltage output,  $i_L$  is the converter output current,  $T_m$  the sampling time,  $L_f$  the passive filter inductance,  $v_L$  the load voltage and  $R_f$  the passive filter resistance.

### B. APF operation mode

By following the same procedure as the previous section, the following equations arise:

$$v_{R_f} + v_S - v_{conver} + v_{L_f} = 0,$$

$$R_f i_{conver} + v_S - v_{conver} + L_f \frac{d}{dt} i_{conver} = 0, \quad (4)$$

thus,

$$L_f \frac{d}{dt} i_{conver} = -v_{conver} - R_f i_{conver} - v_S. \quad (5)$$

By discretizing (5) we have:

$$i_{conver[n+1]} = \frac{T_m}{L_f} [v_{conver[n]} - v_{S[n]}] + i_{conver[n]} D, \quad (6)$$

where  $v_s$  is the voltage source and  $i_{conver}$  the converter output current.

All the above-mentioned equations will be used for PCC implementation. Moreover, three bridges are used for each phase of the VSI, as shown in Fig. 2 presenting four possible switching state for each phase of the VSI. Each of them has its respective activation's in the circuit and respective output voltages as shown on the Table I. Note that The H-bridge converter used in each phase offers a greater guarantee of continuity in the event of breakdowns in any of the phases and working independently in the case of load variations, which is why the APF has advantages. Also, compared to a multi-level converter, it requires less maintenance due to the smaller number of switches [24].

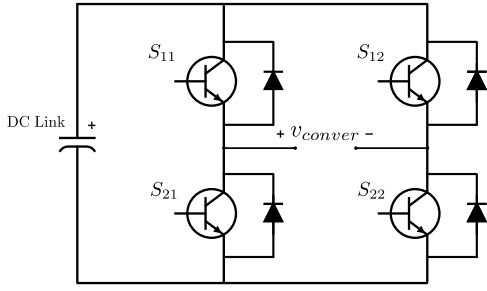


Fig. 2: Two-level H-bridge VSI topology.

TABLE I: Commutation states and outputs for one phase of the converter.

$S_{11}$	$S_{12}$	$S_{21}$	$S_{22}$
0	0	$DC_{link}$	$DC_{link}$
0	$DC_{link}$	$DC_{link}$	0
$DC_{link}$	0	0	$DC_{link}$
$DC_{link}$	$DC_{link}$	0	0

### C. PV system description

Although there are different equivalent circuits for the PV cell depending on the simplifications made within [25], the most commonly used is the equivalent circuit shown in Fig. 3. The  $I(V)$  characteristic of a PV cell is a non-linear equation with multiple parameters classified by those provided by the manufacturers, those known as constants and those that must be computed. Most of the data sheets provided by manufacturers do not provide sufficient information on

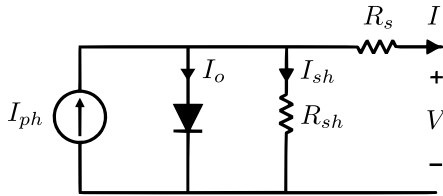


Fig. 3: Equivalent circuit of the PV cell.

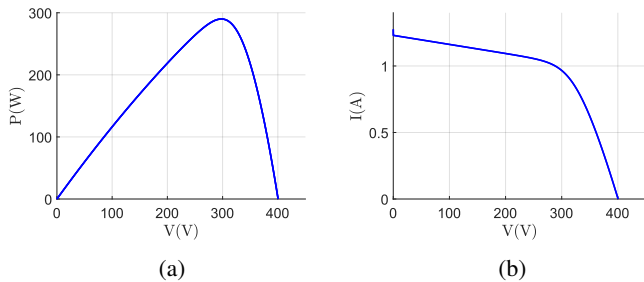


Fig. 4: Simulation results of PV array characteristics. (a) power-voltage, (b) current-voltage.

TABLE II: Characteristics of TWSE-aSi-100W-1 PV module.

$P_{mp}$	99.84 W	$N_s$	159
$I_{mp}$	0.96 A	$n$	1.34
$V_{mp}$	104 V	$k_i$	0.086 A
$I_{sc}$	1.22 A	$K$	1.25e-11
$V_{oc}$	138 V	$q$	1.6e-19
$R_s$	18.33 $\Omega$	$E_{go}$	1.1
$R_{sh}$	471.33 $\Omega$	$IL$	1.26

parameters that depend on weather conditions, such as irradiance and temperature. Therefore, it is necessary to make some assumptions regarding the physical nature of cell behavior in order to establish a mathematical model of the cell and PV module [25]. The equations needed to obtain the output current  $I$  of each PV cell are presented in [26].

Moreover, PV module has a unique current-voltage and power-voltage curve characteristic for each irradiance and temperature conditions. In Fig. 4a the  $P(V)$  characteristics are shown, the parameters of irradiance and temperature used are under the standard test conditions of  $1000 \text{ W/m}^2$  and  $25^\circ \text{C}$  respectively. In the same way, the  $I(V)$  characteristics are presented graphically in Fig. 4b.

From the parameters of the PV panel found in Table II, the simulation of the PV module has been conducted, and used as an energy source for the system. The characteristics of the PV panel have been selected due to the need of the system, using three PV panels in series to achieve the purpose.

### III. PCC DESIGN

The PCC is one of the MPC, where the load current is the control objective. This process can be divided into three stages. First, identifying all the possible switching states, then initialize the optimal switching value and cost function, predict the load currents, calculate the cost function which minimizes the current error on the inverter, and lastly, apply the optimal switching state. Fig 5 shows the diagram of the predictive current controller applied to one phase of the inverter.

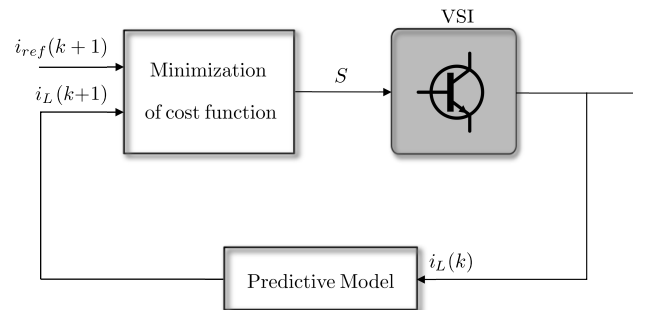


Fig. 5: Diagram of the predictive current controller applied to the two-level VSI.

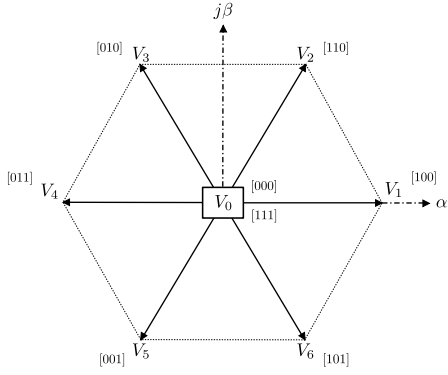


Fig. 6: Space vector diagram for two-level VSI.

This current estimation is made through (8), by introducing the following modification:

$$i_{L_a}[n+1] = \frac{T_m}{L_f} V_{DC} + \left[ 1 - \frac{T_m R_f}{L_f} \right] i_{L_m}[n] + \frac{T_m}{L_f} v_{L_m}[n], \quad (7)$$

$$i_{L_a}[n+1] = \frac{T_m}{L_f} V_{DC} + \left[ 1 - \frac{T_m R_f}{L_f} \right] i_{L_m}[n] - \frac{T_m}{L_f} v_{S_m}[n], \quad (8)$$

being  $i_{L_a}$  the estimated current for phase A,  $i_{L_m}$  the measured current,  $v_c$  the voltage corresponding to a given value of the trigger vector and  $v_{L_m}$  the voltage measured in the load.

#### A. Cost function

The cost function is used to include the desired behavior of the PCC. In this case, the estimation of the output current is performed 4 times in order to consider all possible trigger voltage vectors. The value of the load current is estimated at each sampling time  $T_m$ . All the possible voltage vectors and switching states generated by the VSI are shown in Fig. 6. Then, the trigger vector that provides the lowest value for the cost function is selected and applied during the next sampling time. At each sampling period, the PCC calculates the cost function for each of the possible trigger vectors for each phase of the converter. In this study, the selected cost function is that of the square of the error [6]:

$$f_c = (i_{ref} - i_{L_a})^2, \quad (9)$$

where  $i_{L_a}$  represents the estimated current of phase A while  $i_{L_{ref}}$  is the reference current. For lower cost function values the output current is expected to approximate more closely to the reference current.

## IV. SIMULATION RESULTS

In order to validate the PCC for the dual-mode operation of the VSI, a Matlab/Simulink model of the system has been designed. The electrical parameters of the VSI used for the simulation are the following:  $DC_{link} = 308.8$  V, the frequency of the source  $f_r = 50$  Hz, the filter inductance  $L_f = 45$  mH, the filter resistance  $R_f = 0.2$   $\Omega$ , the load inductance  $L_l = 50$  mH, the load resistance  $R_l = 76.5$   $\Omega$ , and the parameters of the semiconductor  $R_{onIGBT} = 1$  m $\Omega$ ,

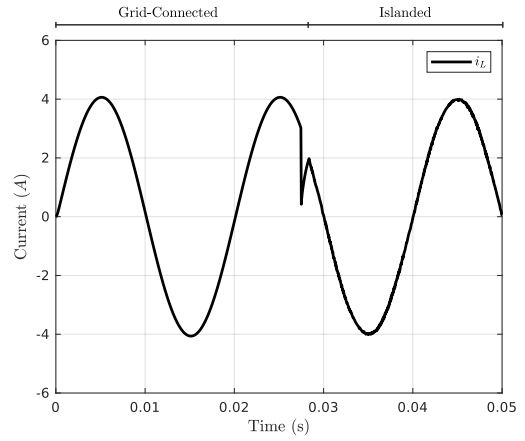


Fig. 7: Load current.

$R_{sIGBT} = 100$  K $\Omega$  and  $C_{sIGBT} = 0.5$  F. Also, for the PCC, a custom MATLAB function is implemented using the following parameters:  $T_m = 45$  ms, to appreciate the continuity of the service in the current after the connection of the VSI the reference used is  $i_{ref} = 4 \angle 0^\circ$  A.

First, the load is grid-connected and the VSI is working as APF. Fig. 7 shows a simulation window of 45 ms where the VSI provides power to the load. Note that the interruption of the grid supply can occur at any time, and this case is happening at  $t = 27.5$  ms. Therefore, the change of functionality of the VSI, occurs at the moment of power breakdown. Initially, the reference current is obtained from the measurement of the reactive power of the system to be compensated. It can be seen from the same figure that the VSI needs about 1 ms to reach the reference.

The reference currents when working as an APF are obtained by means of the Clark and Park transformations. Fig. 8 shows the tracking and the comparison with the reference current in both modes of operation, with the mode of operation switch also occurring at  $T_m = 45$  ms.

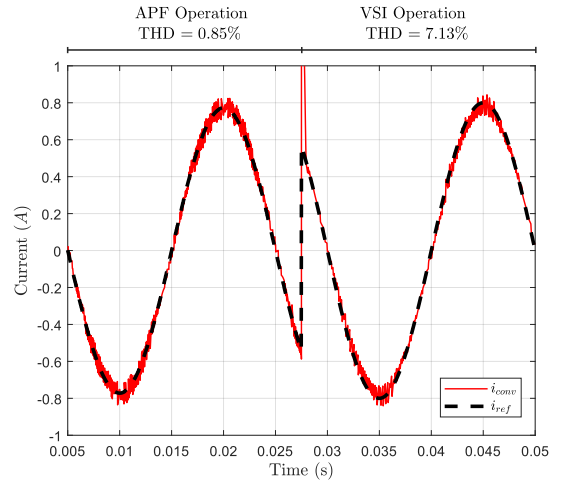


Fig. 8: Current tracking using MPC in the dual-mode converter.

### A. APF results

Then, when the VSI operation is as an APF, it keeps the reactive power at zero. In this case, it has been reduced from 360 kVAR to 0 kVAR, from the point of view of the grid. Fig. 9 shows the reactive power when the APF is applied to the system at  $t = 0.01$  s. In order to see the time response of the system in case of a sudden change, the APF was exposed to a load change. Therefore, a step in the current tracking can be seen from 0.8 A to 0.97 A. As a consequence, the injected power by the APF has changed from 360 kVAR to 390 kVAR, which can be seen in Fig. 10.

A Fast Fourier Transform (FFT) analysis has been performed in order to evaluate the total harmonic distortion (THD) of the proposed system. Fig. 11 shows an analysis in the converter current when it is operating as an APF. The THD of the injected current is observed from the point of view of the grid supply. The value of current THD observed from the power supply source is 0.85 %. Then, the VSI will be evaluated when it has been used as the power converter, to interconnect the PV to the load.

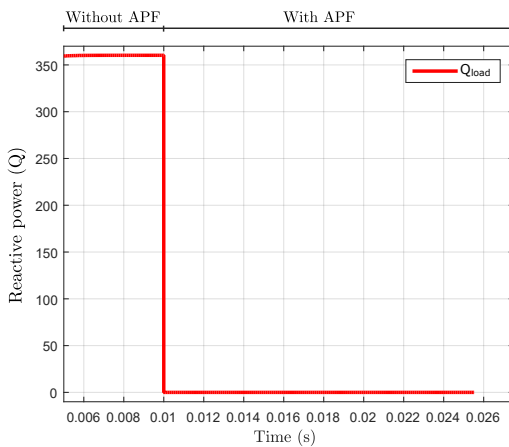


Fig. 9: Reactive power compensation by using the VSI as APF.

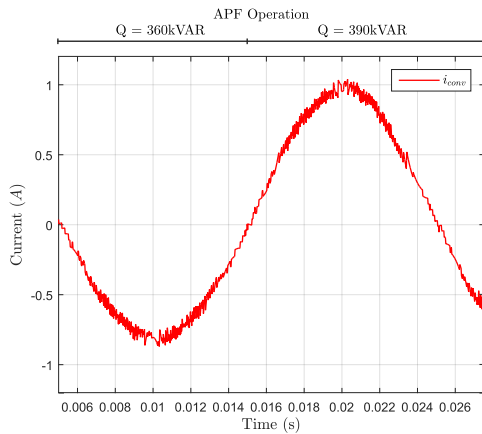


Fig. 10: APF current with change of reactive power.

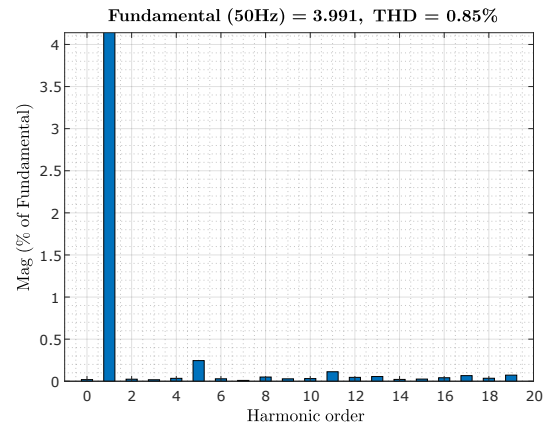


Fig. 11: FFT analysis of the current and THD in the APF.

### B. VSI results

The VSI mode of operation is automatically activated in the case of grid disconnection, remaining in Islanded mode with a power source provided by solar panels.

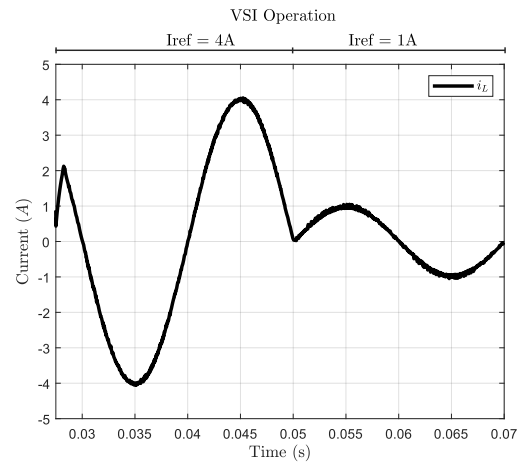


Fig. 12: Load current in VSI mode with change of reference.

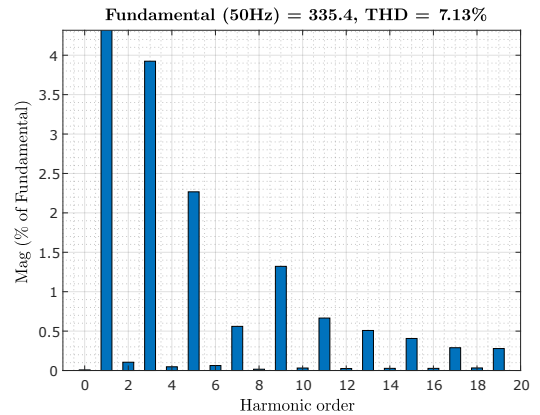


Fig. 13: FFT analysis of the voltage and THD in the VSI.

As in the APF mode of operation, a sudden change of the reference current in the load was made to see the performance of the PCC, from  $4 \angle 0^\circ \text{ A}$  to  $1 \angle 180^\circ \text{ A}$ , as can be seen in Fig. 12.

Lastly, in Fig. 13, an FFT analysis was also conducted to show the THD of the system while working in an islanded power source mode, while feeding the load in isolated form the voltage distortion has a value of 7.13 % with a high percentage of odd harmonics.

## V. CONCLUSION

In this paper, predictive current control of a VSI in dual-mode operation has been presented and validated. Simulation results have shown good tracking response of the proposed control. Therefore, the VSI can successfully work as an APF in the presence of the energy supply and, as VSI managing deliver energy to the load from the PV panels. In both cases, the PCC has a good current tracking. When the VSI is used as APF a low THD is also obtained. However, in the other case, a higher THD was obtained. This latter can be reduced by the introduction of a modulation stage in the proposed PCC.

## ACKNOWLEDGMENT

The authors wish to thank the financial support from the Paraguayan Science and Technology National Council (CONACYT) through the “Maestría en Ingeniería Electrónica” (POSG17-69) and a special thank you to Prof. Julio Pacher for his help.

## REFERENCES

- [1] A. Kumar, B. Sah, A. R. Singh, Y. Deng, X. He, P. Kumar, and R. Bansal, “A review of multi criteria decision making towards sustainable renewable energy development,” *Renewable and Sustainable Energy Reviews*, vol. 69, pp. 596–609, 2017.
- [2] M. I. Mosaad and H. Ramadan, “Power quality enhancement of grid-connected fuel cell using evolutionary computing techniques,” *International Journal of Hydrogen Energy*, vol. 43, no. 25, pp. 11 568–11 582, 2018.
- [3] B. Ren, X. Sun, S. Chen, and H. Liu, “A compensation control scheme of voltage unbalance using a combined three-phase inverter in an islanded microgrid,” *Energies*, vol. 11, no. 9, p. 2486, 2018.
- [4] J. Rodas, R. Gregor, Y. Takase, D. Gregor, and D. Franco, “Multi-modular matrix converter topology applied to the six-phase wind energy generator,” in *2015 50th International Universities Power Engineering Conference (UPEC)*. IEEE, 2015, pp. 1–6.
- [5] J. Rodriguez and P. Cortes, *Predictive control of power converters and electrical drives*. John Wiley & Sons, 2012, vol. 40.
- [6] R. Gregor, L. Comparatore, A. Renault, J. Rodas, J. Pacher, S. Toledo, and M. Rivera, “A novel predictive-fixed switching frequency technique for a cascade h-bridge multilevel statcom,” in *IECON 2016-42nd Annual Conference of the IEEE Industrial Electronics Society*. IEEE, 2016, pp. 3672–3677.
- [7] J. Rodriguez, J.-S. Lai, and F. Z. Peng, “Multilevel inverters: a survey of topologies, controls, and applications,” *IEEE Transactions on Industrial Electronics*, vol. 49, no. 4, pp. 724–738, 2002.
- [8] L. Ning, L. Wanting, Z. Hui, W. Shuzheng, and X. Liansong, “A novel modulation strategy of three level npc converter,” in *2018 13th IEEE Conference on Industrial Electronics and Applications (ICIEA)*. IEEE, 2018, pp. 1347–1351.
- [9] S. Kamran and J. Muñoz, “Study of a state-of-the art m-statcom,” in *2015 IEEE International Conference on Industrial Technology (ICIT)*. IEEE, 2015, pp. 2733–2738.
- [10] F. Gavilan, D. Caballero, S. Toledo, E. Maqueda, R. Gregor, J. Rodas, M. Rivera, and I. Araujo-Vargas, “Predictive power control strategy for a grid-connected 2l-vsi with fixed switching frequency,” in *2016 IEEE International Autumn Meeting on Power, Electronics and Computing (ROPEC)*. IEEE, 2016, pp. 1–6.
- [11] M. V. M. Kumar and M. K. Mishra, “Three-leg inverter-based distribution static compensator topology for compensating unbalanced and non-linear loads,” *IET power electronics*, vol. 8, no. 11, pp. 2076–2084, 2015.
- [12] A. Renault, M. Rivera, L. Comparatore, J. Pacher, J. Rodas, and R. Gregor, “Model predictive current control with neutral current elimination for h-bridge two-level active power filters,” in *2016 IEEE Ecuador Technical Chapters Meeting (ETCM)*, Oct 2016, pp. 1–5.
- [13] M. Huang, Q. Tan, H. Li, and W. Wu, “Improved sliding mode control method of single-phase lcl filtered vsi,” in *2018 9th IEEE International Symposium on Power Electronics for Distributed Generation Systems (PEDG)*. IEEE, 2018, pp. 1–5.
- [14] E.-C. Chang, “Study and application of intelligent sliding mode control for voltage source inverters,” *Energies*, vol. 11, no. 10, p. 2544, 2018.
- [15] S. Buso, S. Fasolo, L. Malesani, and P. Mattavelli, “A dead-beat adaptive hysteresis current control,” *IEEE Transactions on Industry Applications*, vol. 36, no. 4, pp. 1174–1180, 2000.
- [16] A. A. Hossam-Eldin, M. Maghraby, and H. A. Ashour, “Mppt and dead-beat control for power management of hybrid micro-grid applications ahmed. a. hossam-eldin,” *system*, vol. 10, no. 11, p. 12, 2000.
- [17] V. Sabatini, A. Lidozzi, L. Solero, A. Formentini, P. Zanchetta, and S. Bifaretti, “Real-time implicit model predictive control for 3-phase vsi,” in *2018 IEEE Energy Conversion Congress and Exposition (ECCE)*. IEEE, 2018, pp. 4015–4020.
- [18] Z. Yi, A. J. Babqi, Y. Wang, D. Shi, A. H. Etemadi, Z. Wang, and B. Huang, “Finite-control-set model predictive control (fcs-mpc) for islanded hybrid microgrids,” in *2018 IEEE Power & Energy Society General Meeting (PESGM)*. IEEE, 2018, pp. 1–5.
- [19] R. Guzman, L. G. de Vicuña, A. Camacho, J. Miret, and J. M. Rey, “Receding-horizon model-predictive control for a three-phase vsi with an lcl filter,” *IEEE Transactions on Industrial Electronics*, vol. 66, no. 9, pp. 6671–6680, 2018.
- [20] H. J. Fard, “Design and implementation of predictive controllers on the rectifier and quasi impedance-source inverter in a wind energy conversion system based on permanent magnet synchronous generator,” *International Journal on Smart Sensing & Intelligent Systems*, vol. 10, no. 2, 2017.
- [21] C. N. Mukundan and P. Jayaprakash, “Cascaded h-bridge multilevel inverter based grid integration of solar power with pq improvement,” in *2018 IEEE International Conference on Power Electronics, Drives and Energy Systems (PEDES)*. IEEE, 2018, pp. 1–6.
- [22] P. A. Dahono, “A new control method to reduce low-frequency output current ripples of polyphase rectifiers,” in *2007 Power Conversion Conference-Nagoya*. IEEE, 2007, pp. 1099–1104.
- [23] Y. Liao, J. You, J. Yang, Z. Wang, and L. Jin, “Disturbance-observer-based model predictive control for battery energy storage system modular multilevel converters,” *Energies*, vol. 11, no. 9, p. 2285, 2018.
- [24] L. Comparatore, R. Gregor, J. Rodas, J. Pacher, A. Renault, and M. Rivera, “Model based predictive current control for a three-phase cascade h-bridge multilevel statcom operating at fixed switching frequency,” in *2017 IEEE 8th International Symposium on Power Electronics for Distributed Generation Systems (PEDG)*. IEEE, 2017, pp. 1–6.
- [25] H. Bellia, R. Youcef, and M. Fatima, “A detailed modeling of photovoltaic module using matlab,” *NRIAG Journal of Astronomy and Geophysics*, vol. 3, no. 1, pp. 53–61, 2014.
- [26] L. Morínigo, T. Morel, J. Rodas, and R. Gregor, “Predictive current control for a neutral point clamped inverter considering sic-mosfet as switches and using a photovoltaic power source,” *AEIT International Annual Conference*, 2019.